Left Ventricular Heart Phantom for Wall Motion Analysis

Kerstin Müller, Andreas K. Maier, Peter Fischer, Bastian Bier,
Günter Lauritsch, Chris Schwemmer, Rebecca Fahrig and Joachim Hornegger

***Abstract*—In interventional cardiology, three-dimensional anatomical and functional information of the cardiac chambers, e.g. the left ventricle, would have an important impact on diagnosis and therapy. With the technology of C-arm CT it is possible to reconstruct intraprocedural 3-D images from angiographic projection data. Due to the long acquisition time of several seconds, motion-related artifacts, like blurring or streaks, occur. Therefore, the heart dynamics need to be taken into account in order to improve the reconstruction results. When it comes to the evaluation of different motion estimation and compensation algorithms and techniques of motion analysis, there is still a lack of comparability of the final reconstructions and motion parameters between the research groups. Since the results are heavily dependent on the applied motion pattern and simulation parameters, the experiments are not reproducible. We try to overcome these problems by providing varying left heart ventricle phantom datasets, consisting of projection images as well as extracted surface meshes. Up to now, there are six different datasets available: one with a normal sinus rhythm, one with a normal sinus rhythm and a catheter, one with a lateral wall defect of the ventricle, two with a lateral contraction phase shift and one without any motion. The existing datasets are based on a phantom similar to the 4D XCAT phantom with a contrasted left ventricle, myocardium, and aorta. The geometry calibration and acquisition protocol from a real clinical C-arm scanner are used. A webpage is provided where the data and the necessary files are publicly available for download at *conrad.stanford.edu/data/heart*.**

I. Introduction

A. Purpose of the work

The 3-D reconstruction and analysis of cardiac chambers using C-arm CT (rotational angiography) is a challenging field of research. During a rotational acquisition with a C-arm system, the heart chambers, e.g. the left ventricle, are contrasted. Due to the long acquisition time of several seconds, motion-related artifacts occur, for example blurring or streaks, when applying a conventional standard FDK reconstruction algorithm [1]. Therefore, the cardiac motion needs to be integrated into the reconstruction process. In order to allow for comprehensive evaluation of different algorithms, we provide different phantom models with various contraction abilities. For each phantom model, the monochromatic and polychromatic 2-D projection images, as well as pre-processed, i.e. redundancy weighted, cosine weighted, and ramp filtered, projection images are available. The geometry as well as the linear relative heart phases are provided. Furthermore, dynamic surface meshes are generated to enable wall motion analysis and different kinds of motion estimation algorithms.

K. Müller, A. Maier, P. Fischer, C. Schwemmer and J. Hornegger are with the Pattern Recognition Lab, Department of Computer Science and the Erlangen Graduate School in Advanced Optical Technologies (SAOT), Friedrich-Alexander-Universität Erlangen-Nürnberg, Erlangen, Germany. Email:kerstin.mueller@cs.fau.de. B. Bier is with the Pattern Recognition Lab, Department of Computer Science, Friedrich-Alexander-Universität Erlangen-Nürnberg, Erlangen. G. Lauritsch is with the Siemens AG, Healthcare Sector, Forchheim, Germany. R. Fahrig is with the Department of Radiology, Stanford University, Stanford, CA, USA.

B. State-of-the-Art

Several phantoms, either physical phantoms [2] or numerical phantoms, which depict realistic anatomy [3], exist. Some phantoms also model different artifact sources like heart or breathing motion [4]. They all allow a qualitative and quantitative evaluation, but the generation of the projection data varies and does not always reflect realistic acquisition scenarios.
One existing online platform already provides projection images for cardiac vasculature [5]. However, algorithms dealing with the motion from cardiac chambers suffer from different artifacts compared to the coronary arteries and hence different algorithms need to be developed and tested accordingly.

II. Left Ventricular Heart Phantom

A. Coordinate Systems and Transforms

The origin of the 3-D world-coordinate system is set to the C-arm iso-center and the space unit is set to millimeter. The basic geometrical relationship of a voxel $\boldsymbol{x} \in \mathbb{R}^3$ in world-coordinates and a pixel $\boldsymbol{u} \in \mathbb{R}^2$ of the i-th projection image is described by a 3×4 projection matrix $\boldsymbol{A}_i$ in homogenous coordinates [6]:

$$\boldsymbol{A}_i \cdot \begin{pmatrix} \boldsymbol{x} \\ 1 \end{pmatrix} \cong \tilde{\boldsymbol{u}}_i = \begin{pmatrix} u_{i,1} \\ u_{i,2} \\ u_{i,3} \end{pmatrix}, \tag{1}$$

$$\boldsymbol{u}_i = \begin{pmatrix} u_{i,1}/u_{i,3} \\ u_{i,2}/u_{i,3} \end{pmatrix}, \tag{2}$$

where $\tilde{\boldsymbol{u}}_i$ denotes the pixel coordinate in homogenous coordinates. An illustration of the projection geometry is given in Figure 1. S denotes the X-ray source, D the detector plane and O denotes the origin of the image plane.

B. 4D XCAT-based Phantom Datasets

For the simulation of the anatomy and motion pattern of the phantom, the 4-D XCAT phantom [3], [4] is used. The phantom is based on 4-D tagged magnetic resonance imaging data and 4-D high-resolution respiratory-gated CT data of human subjects. In Figure 2a and 2b the anterior and left

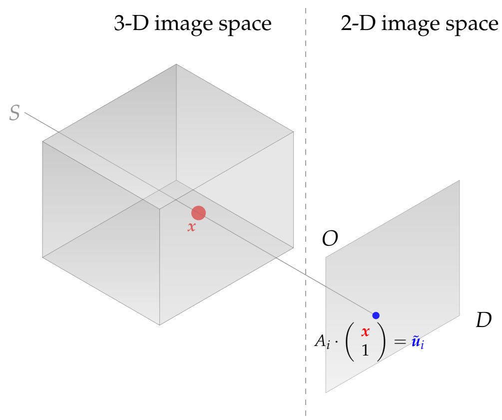

Figure 1: Scheme of the projection geometry.

sagittal view of one generated phantom dataset is shown. Up to now, two different absorption models are simulated, monochromatic and polychromatic absorption.

1) Monochromatic Phantom: Based on the assumption that all materials have the same absorption as water, the left ventricle's bloodpool density was set to 2.5 g/cm^3(1500 HU), the density of the myocardium wall to 1.5 g/cm^3 (500 HU) and the blood in the aorta to 2.0 g/cm^3 (1000 HU). The density of the other materials is set to densities similar to the FORBILD phantom[1].

2) Polychromatic Phantom: A source spectrum $E(b)$ with $b \in [1, 36]$ from 10 keV to 90 kvp peak voltage and a time current product of 2.5 mAs per X-ray pulse was simulated. The bones and the bone marrow, have the material properties according to the mass attenuation coefficients of the NIST X-Ray Table[2]. For all other structures it is assumed that they have the same absorption behavior as water with different densities similar to the FORBILD phantom[1]. The density of the ventricular bloodpool, myocardium and aorta is the same as in the monochromatic simulations from Subsection II-B1. Additionally, it is possible to simulate a catheter coming from the aorta into the left ventricle. The catheter has the material properties of copper[2] and moves according to the heart motion.

C. Projection Generation

The 2-D projections are generated with a real acquisition scenario and geometry calibration from a clinical angiographic C-arm system. The simulated protocol is a clinically available protocol for cardiac procedures. The acquisition time is set to 5 s with 133 projection images covering 200°. The projection images have a dimension of 1240×960 pixels with an isotropic resolution of 0.31 mm/pixel. The distance from source to detector is about 120 cm and from source to iso-center about 80 cm. The generation is based on ray casting as described in [7]. The path segments through the different materials of the scene are determined and the absorption model is evaluated according to Lambert-Beer's Law [8]. A more detailed description of the projection generation can be found in Maier et al. [9]. The projection matrices, as described in Section II-A, were obtained from an offline calibration procedure. An example of a simulated monochromatic and polychromatic 2-D projection image is given in Fig. 2c and Fig. 2d.

D. Surface Mesh Generation

Surface triangle left ventricle (LV) meshes can be generated due to the used analytic spline model [9], which describes the 3-D left ventricle anatomy as well as the motion path. The splines can be sampled at any number of points. In our experiments, we sampled the spline at about 2500 surface points. In Figure 2e and 2f, triangulated LV surface meshes are illustrated.

E. Cardiac Motion Defect Integration

As described in [9], a spline is used to model the 4-D motion. For every normalized time point $t \in [0, 1]$ of the whole scan there exists a 2-D spline surface $\boldsymbol{s} \in [0, 1]^2$. Each spline is defined by control points $\boldsymbol{c} \in \mathbb{R}^2$ with a one-to-one mapping from 3-D coordinates $\boldsymbol{C} \in \mathbb{R}^3$ to the 2-D control points $\boldsymbol{c}$ given by the XCAT phantom [4]. In order to incorporate a motion defect, a region in which the motion is pathological has to be defined. Up to now, we do this using a box $\mathcal{B}$ within the coordinate system of the heart, i.e. a local coordinate system where the z-axis is aligned with the long axis of the heart. Each spline control point $\boldsymbol{C}$ is clipped against the volume $\mathcal{B}$, generating a list $\mathcal{C}_{path}$ of control points inside the pathological volume, where the complete set of all control points is denoted as $\mathcal{C}$. During the tessellation procedure $T(\boldsymbol{s}, t) : \mathbb{R}^2 \to \mathbb{R}^3$, the 2-D spline surface points $\boldsymbol{s}$ are assigned to a 3-D coordinate $\boldsymbol{x}(t) = T(\boldsymbol{s}, t)$. This is done for each normalized time point t of the whole scan. In order to have a smooth transition between $\mathcal{B}$ and the healthy LV surface, a flexibility parameter σ is introduced, where a larger value of σ results in a smooth defect, while a small value yields sharp transitions between pathological and normal tissue. The model incorporates two kinds of motion defects: akinetic and dyskinetic wall motion. The akinetic motion defect prevents contraction or inward motion of the heart in the affected area. A dyskinetic motion is a contradictory movement of the heart, here a delay in the heart motion is introduced. The motion defects can be controlled by a phase shift parameter $\delta \in [0, 1]$. The deformed 3-D coordinate can then be computed as

$$\boldsymbol{x}_{path}(t) = (1 - w(\boldsymbol{s}, t)) \cdot T(\boldsymbol{s}, t) + w(\boldsymbol{s}, t) \cdot T(\boldsymbol{s}, t - \delta), \quad (3)$$

$$w(\boldsymbol{s}, t) = \frac{\sum_{\boldsymbol{c} \in \mathcal{C}_{path}} w'(\boldsymbol{s}, \boldsymbol{c}, t)}{\sum_{\boldsymbol{c} \in \mathcal{C}} w'(\boldsymbol{s}, \boldsymbol{c}, t)}, \quad (4)$$

$$w'(\boldsymbol{s}, \boldsymbol{c}, t) = e^{-\frac{1}{2\sigma^2}||\boldsymbol{s} - \boldsymbol{c}||_2^2}. \quad (5)$$

The Gaussian basis function $w'(\boldsymbol{s}, \boldsymbol{c}, t)$ gives a small weight to control points far away from the current spline surface point $\boldsymbol{s}$ and a higher weight to close control points. Effectively,

[1] http://www.imp.uni-erlangen.de/forbild

[2] http://physics.nist.gov/PhysRefData/Xcom/html/xcom1.html

$\boldsymbol{x}_{path}(t)$ is a linear combination between the transformed spline point $\boldsymbol{s}$ at the current time t and at a time point $t-\delta$. An akinetic motion defect can be realized by setting $\delta = t-t_0$. In our experiments, we set $t_0 = 0$. Hence, the magnitude of the motion in the pathological volume is minimal compared to the motion of the remaining LV. A dyskinetic defect models a shift in the motion phase. This is achieved by setting δ to a fixed value, given as percentage of the heart cycle. Consequently, $\boldsymbol{x}_{path}(t)$ is generated from the transformed spline points at the current time and at an earlier time with a fixed phase shift. As a result, the motion in the pathological volume is delayed compared to the motion of the remaining LV.

F. Clinical Parameters

In order to classify the relation between the motion defects described in Section II-E and pathological effects, two clinical parameters are used: the ejection fraction (EF) and the systolic dyssynchrony index (SDI):

a) Ejection Fraction: The ejection fraction (EF), is the fraction of the blood volume that is ejected with each heart beat. The end-diastolic volume (EDV) and end-systolic volume (ESV) are used to compute the EF

$$\mathrm{EF}[\%] = 100 \cdot \frac{\mathrm{EDV} - \mathrm{ESV}}{\mathrm{EDV}}. \tag{6}$$

A normal EF has a lower limit of $\sim$50 %, below that the contraction ability of the LV is impaired [10].

b) Systolic Dyssynchrony Index (SDI): The systolic dyssynchrony index (SDI) quantifies the mechanical dyssynchrony of the LV. It was introduced by Kapatenakis et al. [11] for 3-D echocardiography. The SDI is computed as the standard deviation of the time to maximal contraction among the 16 ventricle segments as recommended by the American Heart Association [12] and is hence an indicator for LV synchrony. In order to allow comparisons between various patients with different heart rates, the SDI is expressed as percentage of the duration of the cardiac cycle rather than in milliseconds [13]. Since the SDI represents the standard deviation between contraction phases, a higher SDI denotes increased ventricular dyssynchrony. For echocardiography, Kapetanakis et al. stated an SDI $\leq 3.5 \pm 1.8$ % as normal [11]. It needs to be mentioned that the SDI is a relatively new measurement technique of dyssynchrony and it still varies between the methods of measurement, e.g. Sachpekidis et al. [14] stated that there exist variations among the methods, but irrespective of the analysis software there is an agreement that healthy individuals rarely have SDI values over 6%.

III. Experiments and Discussion

The accuracy of the generation of the 2-D projection images was already investigated in [9], which showed that the reconstructions performed with the simulated 2-D projections and a sharp kernel have less than 1 HU error. The relation between the introduced pathologies and the clinical parameters are given in Table I. All six phantom datasets can be used to evaluate quantitatively the quality of motion estimation and compensation algorithms (c.f [15], [16]). Furthermore, the phantom surface meshes can be used to evaluate wall motion dyssynchrony. The phantom dataset p_0 is the static phantom with a relative heart phase of 75 %. The normal phantom p_1 without the catheter and the phantom p_5 with the catheter have an SDI of 4.16 % which is in the upper normal range. The two phantoms, p_2 with the induced lateral phase shift $\delta = 0.2$ ($\sigma = 0.1$) and p_3 with $\delta = 0.3$ ($\sigma = 0.1$), are clearly classified to have a moderate or even severe dysfunction. The phantom with the complete lateral wall defect p_4 ($\delta = t-0$, $\sigma = 0.05$) has a slightly increased SDI value and a very low EF.

Table I: Motion defect, heart rate (HR), ejection fraction (EF) and systolic dyssynchrony index (SDI) of the phantom datasets.

Dataset	Motion Defect	HR [bpm]	EF[%]	SDI[%]
p_0	n.a	n.a	n.a	n.a
p_1	none	60	62.37	4.16
p_2	20% [lateral]	60	60.40	6.47
p_3	30% [lateral]	60	53.65	12.74
p_4	0 %[defect lateral]	60	38.70	5.05
p_5	none	60	62.37	4.16

A standard reconstruction using an FDK algorithm [1] with the monochromatic projection data of the static phantom and a relative heart phase of 75 % is shown in Fig. 3a. The FDK reconstruction of the dynamic phantom p_1 is shown in Figure 3b. The defect at the lateral wall of p_4 is visible in the reconstruction in Figure 3c and indicated by the arrow. A reconstruction of p_5 with the polychromatic projections, normal contraction and the simulated catheter is given in Fig. 3d.

IV. Summary and Conclusion

We presented publicly available left ventricle phantom datasets in order to evaluate motion analysis parameter and reconstruction algorithms for C-arm angiography. The major benefit of our projection datasets is the realistic setup and phantom data generation. Furthermore, the surface meshes provide possibilities for specific motion estimation algorithms, as well as to study ventricular wall motion. Up to now, six different projection datasets (monochromatic and polychromatic) that are simulated based on a numerical model consisting of anatomical and physiological data from patient data are available on the webpage (*conrad.stanford.edu/data/heart*).

Acknowledgment

The authors gratefully acknowledge funding support from the NIH grant R01 HL087917 and of the Erlangen Graduate School in Advanced Optical Technologies (SAOT) by the German Research Foundation (DFG) in the framework of the German excellence initiative.

References

[1] L. Feldkamp, L. Davis, and J. Kress, "Practical cone-beam algorithm," *J Opt Soc Am A*, vol. 1, no. 6, pp. 612–619, June 1984.

[2] T. Boltz, W. Pavlicek, R. Paden, M. Renno, A. Jensen, and M. Akay, "An anthropomorphic beating heart phantom for cardiac X-ray CT imaging evaluation," *J Appl Clin Med Phys*, vol. 11, no. 1, January 2010.

[3] W. Segars, M. Mahesh, T. Beck, E. Frey, and B. Tsui, "Realistic CT simulation using the 4D XCAT phantom," *Med Phys*, vol. 35, no. 8, pp. 3800–3808, August 2008.

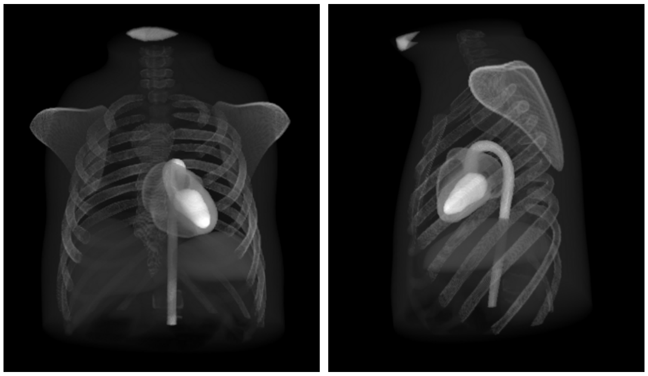

(a) Anterior view of the polychromatic generated phantom dataset with the catheter.

(b) Left sagittal view of the polychromatic generated phantom dataset with the catheter.

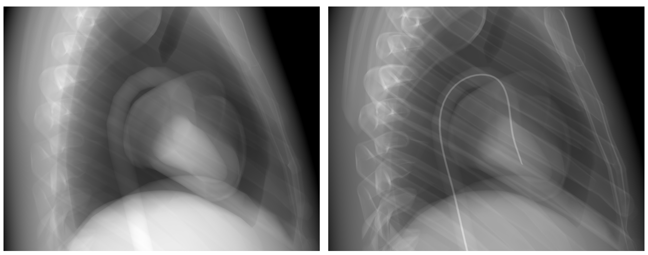

(c) Simulated 2-D projection image, with contrasted LV, myocardium and aorta.

(d) Simulated 2-D projection image of catheter phantom.

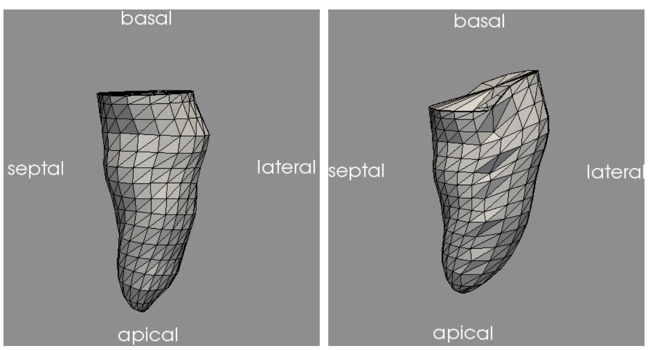

(e) Generated triangle mesh of the left ventricle with normal contraction.

(f) Generated triangle mesh of the left ventricle with wall defect.

Figure 2: Example images of the available phantom datasets.

[4] W. Segars, D. Lalush, and B. Tsui, "A realistic spline-based dynamic heart phantom," *IEEE Trans Nucl Science*, vol. 46, no. 3, pp. 503–506, June 1999.

[5] C. Rohkohl, G. Lauritsch, A. Keil, and J. Hornegger, "CAVAREV-an open platform for evaluating 3D and 4D cardiac vasculature reconstruction," *Phys Med Biol*, vol. 55, pp. 2905–2915, May 2010.

[6] R. Hartley and A. Zisserman, *Multiple View Geometry in Computer Vision*, 2nd ed., Cambridge, Ed. Cambridge University Press, 2004.

[7] H. Scherl, "Evaluation of state-of-the-art hardware architectures for fast cone-beam CT reconstruction," Ph.D. dissertation, Friedrich-Alexander-Universität Erlangen-Nürnberg, 2011.

[8] T. Buzug, *Computed Tomography From Photon Statistics to Modern Cone-Beam CT*. Springer Verlag, 2008.

[9] A. Maier, H. Hofmann, C. Schwemmer, J. Hornegger, A. Keil, and R. Fahrig, "Fast simulation of X-ray projections of spline-based surfaces using an append buffer," *Phys Med Biol*, vol. 57, no. 19, pp. 6193–6210, October 2012.

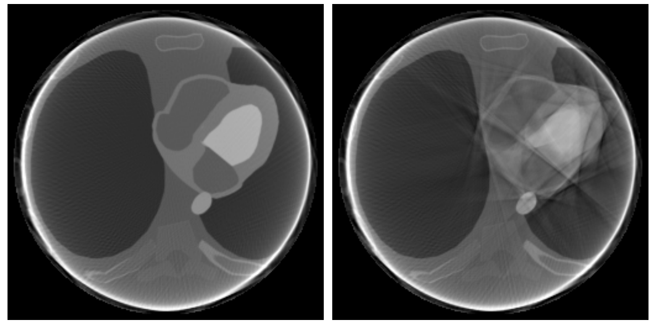

(a) Standard FDK reconstruction of the static phantom and a relative heart phase of 75%.

(b) Standard FDK reconstruction of the dynamic phantom.

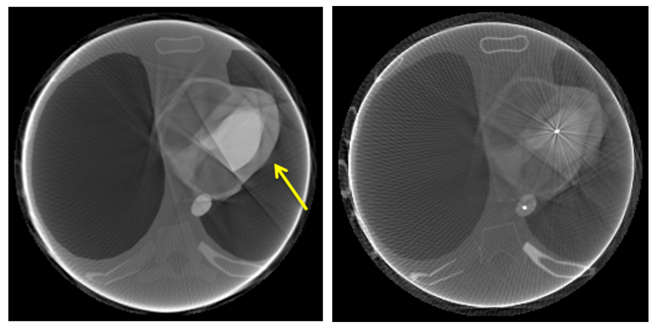

(c) Standard FDK reconstruction of the phantom with an introduced lateral wall defect.

(d) Standard FDK reconstruction of the polychromatic phantom with the simulated catheter.

Figure 3: Example reconstructions of the available monochromatic and polychromatic phantom datasets.

[10] M. Pfisterer, A. Battler, and B. Zaret, "Range of normal values for left and right ventricular ejection fraction at rest and during exercise assessed by radionuclide angiocardiography," *Eur Heart J*, vol. 6, no. 8, pp. 647–655, August 1985.

[11] S. Kapetanakis, M. Kearney, A. Siva, N. Gall, M. Cooklin, and M. Monaghan, "Real-time three-dimensional echocardiography a novel technique to quantify global left ventricular mechanical dyssynchrony," *Circulation*, vol. 112, no. 7, pp. 992–1000, August 2005.

[12] M. D. Cerqueira, N. J. Weissman, A. K. Dilsizian, V.and Jacobs, S. Kaul, W. K. Laskey, and et al., "Standardized myocardial segmentation and nomenclature for tomographic imaging of the heart," *Circulation*, vol. 105, no. 4, pp. 539–542, January 2002.

[13] V. Gimenes, M. Vieira, M. Andrade, J. Pinheiro Jr, V. Hotta, and W. Mathias Jr, "Standard values for real-time transthoracic three-dimensional echocardiographic dyssynchrony indexes in a normal population," *J Am Soc Echocardiog*, vol. 21, no. 11, pp. 1229–1235, November 2008.

[14] V. Sachpekidis, A. Bhan, and M. Monaghan, *Textbook of Real-Time Three Dimensional Echocardiography*, L. Badano, R. Lang, and J. Zamorano, Eds. Springer-Verlag London Limited, 2011.

[15] K. Müller, C. Schwemmer, J. Hornegger, Y. Zheng, Y. Wang, G. Lauritsch, A. Maier, C. Schultz, and R. Fahrig, "Evaluation of interpolation methods for surface-based motion compensated tomographic reconstruction for cardiac angiographic C-arm data," *Med Phys*, vol. 40, no. 3, pp. 031 107–1 –12, March 2013.

[16] K. Müller, C. Schwemmer, G. Lauritsch, C. Rohkohl, A. Maier, H. Heidbüchel, S. De Buck, D. Nuyens, Y. Kyriakou, C. Köhler, R. Fahrig, and J. Hornegger, "Image artifact influence on motion compensated tomographic reconstruction in cardiac C-arm CT," in *Fully 3D 2013 Proceedings*, 2013.